Phase-error correction for multiple planes using a sharpness metric

Abbie E. Tippie and James R. Fienup*

The Institute of Optics, University of Rochester, Rochester, New York 14627, USA
**Corresponding author: fienup@optics.rochester.edu*

Received October 20, 2008; revised January 19, 2009; accepted January 30, 2009; posted February 5, 2009 (Doc. ID 102943); published February 27, 2009

Phase errors in multiple planes create an anisoplanatic (space-variant) blur in an image. We show how phase errors in multiple planes can be corrected with the use of a sharpness metric for heterodyne or holographic imaging. We derive the theoretical framework necessary for this anisoplanatic imaging situation. A digital simulation and results are presented. We demonstrate the success of this nonlinear optimization technique for phase errors in two planes. © 2009 Optical Society of America

OCIS codes: 090.1000, 100.3010, 100.3020, 090.1995, 100.3190, 010.1330.

Imaging through multiple planes of optical aberrations occurs in a variety of scenarios such as atmospheric turbulence (particularly for horizontal paths) [1], biological tissue [2], other random media, and space-variant optical systems. Sharpness metrics were first used for incoherent imaging through atmospheric turbulence using telescopes [3]. Following that work, several others have applied sharpness metrics to correcting motion-induced, 1-D phase errors in synthetic aperture radar problems [4–6]. Recent research has explored various sharpness metrics and their performance in correcting 2-D phase errors in digital holography [7]. In all these previous cases, the phase errors could be approximated as being in one plane near the pupil of the telescope or detection plane, and the aberrations were space invariant. Thurman and Fienup [8] demonstrated the correction of space-variant phase errors (the anisoplanatic case) caused by a single phase screen a distance from the aperture. That approach could not correct multiple phase screens. In this Letter, we extend that work to incorporate correction of aberrations in multiple planes.

For the process of simulating the digital hologram with aberrations, we follow the method outlined in [7,8] and reconstruct the aberrated field, $G(x,y)$, from the object. Alternatively, one may perform heterodyne detection or record three or more on-axis holograms with different constant phases associated with the reference beam and use standard phase-shifting techniques. By inverting $G(x,y)$ while compensating for the aberrations, we can compute an image, $f(\xi,\eta)$, of the optical field scattered by the object in the nominal object plane. In this Letter, we use different speckle realizations of the fields, assuming an optically rough object. This can be implemented experimentally by slightly rotating or translating the object between exposures, assuming that the aberrations are fixed during the entire data collection time. The speckle-reduced image intensity is then the average of the magnitude-squared image fields,

$$I(\xi,\eta)=\frac{1}{K}\sum_{k=1}^{K}|f_k(\xi,\eta)|^2, \tag{1}$$

where K is the number of speckle realizations.

We consider a case for which there is a volume of phase errors between the object and the hologram plane. Simulating the extended media as a collection of thin phase screens that are located at different distances within the total propagation length can be a good approximation. For the present discussion, we examine the case in which the phase errors are located solely in the object beam path and the reference beam is ideal. We ignore aberrations in the beam illuminating the object, since the rough object will impose a random phase on the illuminating beam. We wish the digital transverse sample spacing to remain the same, so we implement the propagation between phase screens using angular-spectrum propagation, given in the paraxial regime for a given field $g(x,y)$ over a distance z as

$$\mathcal{A}[z;g(x,y)]=\mathcal{F}^{-1}\{\mathcal{F}[g(x,y)]\exp[-i\pi\lambda z(f_x^2+f_y^2)]\}, \tag{2}$$

where $\mathcal{F}$ denotes a Fourier transform and we have ignored inconsequential constants.

Figure 1 depicts the holography setup and optical propagation paths, where z_1 is the distance from the object plane to the first plane of phase error, z_p is the distance from the $(p-1)$th phase plane to the pth phase plane, φ_p is an estimate of the phase error for the pth plane, P is the number of phase screens, and $G_k(u,v)$ is the kth aberrated field in the hologram plane. To simplify later notation, we define a forward propagator

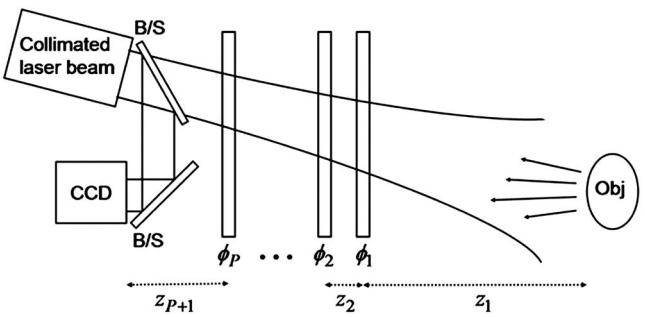

Fig. 1. Layout for recording a digital hologram with multiple planes of phase error present.

0146-9592/09/050701-3/$15.00

$$\mathcal{P}_{1\to p\_}[f_k(\xi,\eta)] = \mathcal{A}\{z_p;\exp(i\varphi_{p-1})\cdots\mathcal{A}[z_3;\exp(i\varphi_2)\times\mathcal{A}\{z_2;\exp(i\varphi_1)\mathcal{A}[z_1;f_k(\xi,\eta)]\}]\cdots\}. \quad (3)$$

The inverse propagator from the hologram plane can be written in a similar fashion,

$$\mathcal{P}^{\dagger}_{P+1\to p\_}[G_k(u,v)] = \exp(-i\varphi_p)\mathcal{A}(-z_{p+1};\times\exp(-i\varphi_{p+1})\cdots\exp(-i\varphi_{P-1})\times\mathcal{A}[-z_P;\exp(-i\varphi_P)\times\mathcal{A}\{-z_{P+1};G_k(u,v)\}]\cdots). \quad (4)$$

Using the above definitions, the aberrated field in the hologram plane can be written as $G_k(u,v)=P_{1\to P+1}[f_k(\xi,\eta)]$. Likewise, using the inverse propagator, the image field is $f_k(\xi,\eta)=P^{\dagger}_{P+1\to 1}[G_k(u,v)]$, where for brevity we are ignoring the finite extent of the recorded hologram.

To estimate and correct for the phase errors present in the object-beam propagation path, we maximize the sharpness metric

$$S = \sum_{\xi,\eta} I^{\beta}(\xi,\eta) - \alpha\sum_{k=1}^{K}\sum_{f_\xi,f_\eta} M(f_\xi,f_\eta)|F_k(f_\xi,f_\eta)|^2 \quad (5)$$

as a function of the phase estimates, where α and β are constants, $F_k(f_\xi,f_\eta)$ is the Fourier transform of $f_k(\xi,\eta)$, and $M(f_\xi,f_\eta)$ is a weighting function that defines the spatial frequency content of the object fields that are sensed over the area of the digital hologram. The first term is a standard sharpness metric. The second term penalizes frequency content of the image field that could not have come from the digital hologram through reasonable atmospheric turbulence. We found that including a constraint for the frequency content was important to achieve successful image reconstruction by avoiding phase screens that constituted telescopes demagnifying the image (thereby increasing the sharpness). We chose to constrain the Fourier domain, since the frequency content of the object will remain approximately constant throughout the propagation distance, even in the presence of reasonable phase aberrations.

We used a conjugate-gradient routine to maximize the metric as a function of estimates of the phase screens. The partial derivative of S with respect to the value of the phase in screen p at location (x,y) can be written in a fashion similar to Eq. (41) in [9], in terms of the hologram and image fields, as

$$\frac{\partial S}{\partial\varphi_p(x,y)} = \frac{2}{K}\sum_{k=1}^{K}\mathrm{Im}(P_{1\to p\_}[\beta I^{\beta-1}(\xi,\eta)f_k(\xi,\eta)]\times\{P^{\dagger}_{P+1\to p}[G_k(u,v)]\}^{*}) - \frac{2\alpha}{K}\sum_{k=1}^{K}\mathrm{Im}(P_{1\to p\_}\{\mathcal{F}^{-1}[M(f_\xi,f_\eta)F_k(f_\xi,f_\eta)]\}\times\{P^{\dagger}_{P+1\to p}[G_k(u,v)]\}^{*}). \quad (6)$$

Since an atmospheric phase is smooth, we chose polynomial phase estimates,

$$\varphi_p(x,y) = \sum_j c_{p,j}\psi_j(x,y), \quad (7)$$

where j is the index for the basis function $\psi_j(x,y)$ and $c_{p,j}$ are the expansion coefficients. We optimized over the coefficients $c_{p,j}$, for which the partial derivatives are

$$\frac{\partial S}{\partial c_{p,j}} = \sum_{x,y}\psi_j(x,y)\frac{\partial S}{\partial\varphi_p(x,y)}. \quad (8)$$

Our starting guess for each coefficient was zero. We then performed five conjugate gradient (CG) iterations using the third-order polynomials terms and five more iterations adding fourth-order terms and repeated five more CG iterations for each additional higher-order term up to the 15th-order polynomial terms, similar to what was done in [7].

Individual speckle realizations were simulated by multiplying the square root of the object intensity by a zero-mean, circular complex Gaussian-distributed random variable. To avoid aliasing and wrap-around effects in our digital simulation, we limit the angular extent of the field propagated from the object by cropping out higher spatial frequencies but left the angular extent wide enough to illuminate an area larger than the detector. The spatial frequency content of the image is determined by considering the pixel pitch of the detector Δx, the total array size N, distance of propagation z, and the laser illumination wavelength λ. For the simulations presented in this paper, $N=256$, $D=N\Delta x=16$ cm, $\lambda=514$ nm, and $z=500$ m. We employed $K=24$ speckle realizations. For our forward propagation model, an array larger than our detector size was used.

The aberrations are assumed to be constant during the collection of all the speckle realizations. The phase screens used in this simulation are 15th-order polynomial approximations for atmospheric phase screens [10]. The effective D/r_0 [11] of both phase screens is 10. The phase screens were spaced equidistant throughout the propagation distance such that $z_1=z_2=z_3=166.6$ m.

The support of the mask was created by taking the Fourier transform of $G_1(u,v)$, the aberrated field in the hologram plane for one of the speckle realizations, and defining a square that captured most of its energy. $M(f_\xi,f_\eta)$ is set to zero inside the square and unity outside the square. A cosine guard band is used as a gradual transition between regions. By testing a few different values for the scaling constant α, 5×10^{-8} was chosen for the simulations presented here. For the sharpness metric term, we chose β equal to 1.01. More work could be done to optimize α, β, and the size of the mask to achieve better image-reconstruction results.

The ability to successfully reconstruct images by using our sharpness algorithm for multiple planes is shown in Fig. 2. Figure 2(a) shows the ideal image. Figure 2(b) shows the image when the phase screens are present in the system without correction. The ab-

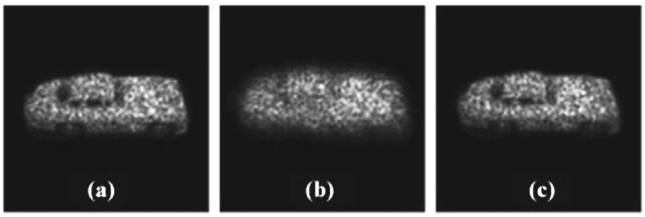

Fig. 2. Image reconstruction results using two phase screens. (a) The ideal image. Two-screen simulation when (b) there is no aberration correction and (c) the phase estimates have been used in the reconstruction.

errated image is a poor visual representation of the ideal image. However, once we have estimated the phase screens and used them to reconstruct and image by inverse propagation, we obtained an image shown in Fig. 2(c), having greatly improved quality.

To quantify the results of our phase-error correction, we computed the absolute normalized rms error of the reconstructed image with respect to the ideal image [12,13]. For the aberrated images, the absolute error was 0.3368. Upon reconstruction, the absolute error improved to 0.1804. Successful image reconstruction depends on multiple parameters, including number of speckle realizations, type and contrast of the object, distance between phase screens, location of phase screens with respect to the object location and detector location, magnitude of the aberrating phase, and signal-to-noise ratio. As in [7] we expect this approach to be relatively insensitive to noise. Figure 3 shows the magnitude of the field backpropagated to the image (on the left) from the detector (on the right). Figures 3(e)–3(h) show an enlarged portion of vertical and horizontal slices near the image. Although we can see differences in the propagation of individual speckles, Fig. 2 shows that we are able to reconstruct a reasonably good image with similar speckles.

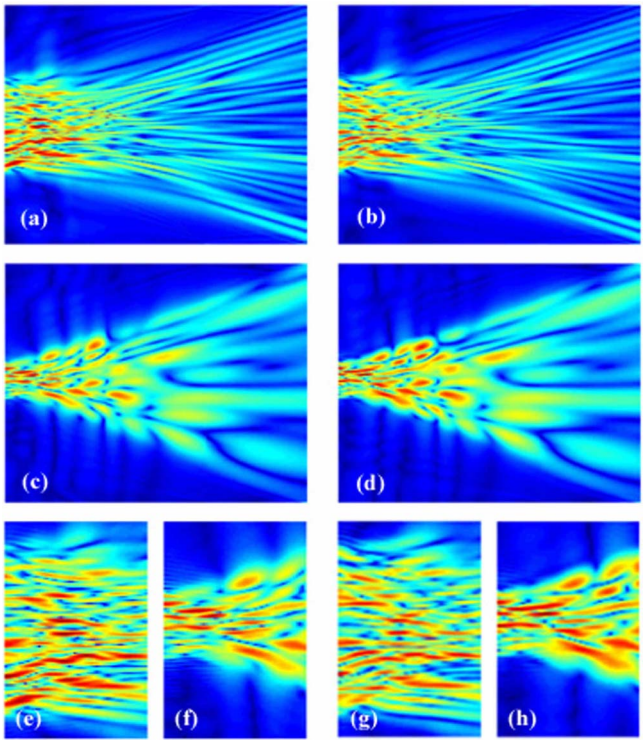

Fig. 3. (Color online) Field magnitude versus z from the image to the detector (left to right); each pair: truth and reconstructed. (a), (b) Horizontal slice; (c), (d) vertical slice; and (e)–(h) magnified slices of (a), (c), (b), and (d) near the image.

We have successfully demonstrated the ability to reconstruct images from digital holography data when multiple planes of aberrations are present, causing anisoplanatic blurring. Image reconstruction has been shown for two planes of optical aberrations. Good reconstruction results under heavily nonisoplanatic conditions is a significant advance. Future research will include optimization of the two-screen case for increased robustness, extending it to a greater number of phase screens to more accurately model volume atmospheric turbulence, developing an understanding of performance as a function of the statistics of the object and imaging scenario, and laboratory experiments to verify the simulations presented in this Letter.

References

1. L. C. Andrews and R. L. Phillips, *Laser Beam Propagation through Random Media* (SPIE Press, 2005).
2. A. Ishimaru, *Wave Propagation and Scattering through Random Media* (Academic, 1978).
3. R. A. Muller and A. Buffington, J. Opt. Soc. Am. **64**, 1200 (1974).
4. R. G. Paxman and J. C. Marron, Proc. SPIE **976**, 37 (1988).
5. F. Berizzi and G. Corsini, IEEE Trans. Aerosp. Electron. Syst. **32**, 1185 (1996).
6. J. R. Fienup and J. J. Miller, J. Opt. Soc. Am. A **20**, 609 (2003).
7. S. T. Thurman and J. R. Fienup, J. Opt. Soc. Am. A **25**, 983 (2008).
8. S. T. Thurman and J. R. Fienup, J. Opt. Soc. Am. A **25**, 995 (2008).
9. J. R. Fienup, Appl. Opt. **32**, 1737 (1993).
10. R. G. Lane, A. Glindemann, and J. C. Dainty, Waves Random Media **2**, 209 (1992).
11. M. C. Roggemann and B. M. Welsh, *Imaging through Turbulence* (CRC Press, 1996).
12. J. R. Fienup, Appl. Opt. **36**, 8352 (1997).
13. M. Guizar-Sicairos, S. T. Thurman, and J. R. Fienup, Opt. Lett. **33**, 156 (2008).